# CT of the Airways

Michael Trojan, Hans-Ulrich Kauczor,
Claus Peter Heußel, and Mark Oliver Wielpütz

## Contents



**Abstract**

Multidetector computed tomography (MDCT) is the method of choice for morphological imaging of the airways and associated diseases. High isotropic resolution and high contrast are the ideal prerequisites to generate multiplanar reformats (MPRs), MinIPs, MIPs, and 3D and even 4D techniques in order to demonstrate the typical findings of airway diseases, such as bronchiectasis, bronchial wall thickening, mucus plugging, tree-in-bud pattern, mosaic attenuation pattern, or air trapping. The main diseases of the airways studied by MDCT include bronchiectasis, cystic fibrosis, asthma, primary ciliary dyskinesia, tracheobronchomalacia, relapsing polychondritis, and bronchiolitis.

M. Trojan (✉) • H.-U. Kauczor • M.O. Wielpütz
Department of Diagnostic and Interventional Radiology and Translational Lung Research Center (TLRC), German Lung Research Center (DZL), University Hospital of Heidelberg, Heidelberg, Germany
e-mail: michael.trojan@med.uni-heidelberg.de; hu.kauczor@med.uni-heidelberg.de; mark.wielpuetz@med.uni-heidelberg.de

C.P. Heußel
Department of Diagnostic and Interventional Radiology with Nuclear Medicine and Translational Lung Research Center (TLRC), German Lung Research Center (DZL), Thoraxklinik gGmbH at University Hospital of Heidelberg, Heidelberg, Germany
e-mail: heussel@uni-heidelberg.de

Med Radiol Diagn Imaging (2017)
DOI 10.1007/174_2017_153, © Springer International Publishing AG
Published Online: 03 November 2017

# 1 Introduction

## 1.1 Radiologic Anatomy of the Airways and Physiology

The airways denote the tubular and branching structures, which supply the lungs with air. They comprise the airways extending from the larynx downwards to the terminal bronchioles. In the context of CT the airways can be subdivided in four major parts: (1) trachea; (2) main stem bronchi; (3) visible segmental and subsegmental bronchi; and (4) the small airways, which—under normal conditions—are not visible by CT due to the restricted resolution. The normal length of edge of each voxel in MDCT is about 250 μm and therefore larger than the smallest lung structures. Consequently, each voxel contains air, lung parenchyma, and blood, resulting in different shades of gray. Airways and structures smaller 2 mm usually cannot be differentiated.

The trachea begins at the inferior margin of the cricoid cartilage and extends for approximately 12 cm to the carina where it bifurcates into the right and left main-stem bronchi. Since the trachea is rather mobile it can change its length in z-axis substantially during respiration. Thus, the carina can move from the level of the upper border of the fifth thoracic vertebra (position during tidal respiration) to the level of the sixth thoracic vertebra during deep inspiration (Standring 2005). 16–20 incomplete horseshoe-shaped cartilages support the anterior and lateral tracheal walls with the open end posteriorly to the adjoining esophagus. The membranous posterior wall (pars membranacea) connects the ends of the incomplete cartilaginous rings. The normal tracheal wall is 1–3 mm thick.

At the level of the carina the main stem bronchi arise from the trachea. The right main stem bronchus is wider, shorter, and has a more vertical course than the left one. This is one of the reasons that aspirations, e.g., of foreign bodies, occur more frequently on the right side. The first branching of the right main stem bronchus—into the upper lobe bronchus and the bronchus intermedius—is still localized within the mediastinum at a distance from the carina of approximately 2.5 cm. After this branching the bronchus intermedius enters the pulmonary hilum and divides into the middle lobe and lower lobe bronchus. The left principal bronchus is narrower, less vertical than the right one and enters the lung before the branch-off of the upper lobe bronchus which occurs at approximately 5 cm distal to the carina from where the lower lobe bronchi supply the lower lobe. As there is no middle lobe on the left side, the lingula is supported by the lingular bronchus, which originates from the left upper lobe bronchus.

The lobar bronchi subsequently divide in a dichotomic manner into segmental and subsegmental bronchi with further bifurcations resulting in a total of approximately 21 generations. In each branching generation the diameters and the wall thickness of the bronchi continuously decrease (Weibel 1963). This observation is also called proximal-to-distal tapering.

The cartilaginous support of the airways is continuously changing over the branching generations. The trachea and extrapulmonary bronchi contain incomplete rings of hyaline cartilage. The intrapulmonary bronchi only contain discontinuous plates or islands of cartilage, the irregularity of which increases with each further branching generation and finally the cartilaginous islands normally disappear when the airway diameter falls below 1 mm.

The small airways, which do not contain cartilage within their walls and with a diameter under 1 mm, are called bronchioles. They represent the 10th–20th generations of airways. They are the smallest and most peripheral, but still purely conducting airways, hence not containing any alveoli in their walls. Distal to the terminal bronchiole there are the acini, which consist of 3–4 generations of respiratory bronchioles leading to 3–8 generations of alveolar ducts finally leading to single alveoli.

The part of the lung distal to a single terminal bronchiole is defined as primary lobule of the lung. The secondary lobule is the smallest functional subsection of the lung surrounded by connective tissue septa and consists of approximately 3–6 primary lobules, representing the smallest functional unit of lung and reproducing it in

miniature (Webb 2006). Secondary lobules have polygonal shapes with each side ranging from 1 to 2.5 cm and are readily discernable on high resolution CT (Weibel and Gomez 1962; Webb 2006). The smallest normal (i.e., healthy) airways visible at CT have a diameter of 2 mm because of the spatial resolution on CT (Burgel et al. 2013), which correspond approximately to the 8–9th generation bronchioli.

Breathing is a periodical process, which is composed of ventilation and respiration. Ventilation describes the movement of air into the lungs. Healthy adults ventilate the lungs with around 500 mL air in average 12 times per minute at rest with a high potential to raise due to physical stress or lung diseases, such as chronic obstructive pulmonary diseases, etc. Under these conditions the ventilation rate can raise up to >30/min. Respiration needs to be differentiated from ventilation. It describes the exchange of gases across the respiratory surfaces through the process of diffusion. The exchange of gas in the alveoli is defined as external respiration, the diffusion of gas between cells and blood as internal respiration.

## 2 Technical Aspects

### 2.1 Scanning Protocol

Nowadays a state-of-the-art MDCT of the thorax yields a volumetric dataset of images with an isotropic sub-millimeter resolution which covers the complete thoracic cavity within a single breath hold; more precisely in less than 10 s, making a breath-hold CT for dyspneic patients feasible (Kauczor et al. 2011). A standard scan is usually carried out in inspiration without intravenous application of contrast medium. The combination of high spatial resolution and volumetric coverage of the lung is mandatory as it results in three-dimensional high resolution CT (3D HRCT). As the airways in the lung parenchyma are high contrast structures intermediate to low dose settings are appropriate. The collimation should be 0.5–1 mm. A pitch of 1–1.4, a tube voltage of 100–120 kV, and a tube current between 50 and 120 mA should be chosen (Kauczor et al. 2011). The automatic exposure control and dose modulation should be switched on. For multiplanar reformats (MPRs) and other post-processing tools overlapping reconstruction is recommended. The reconstructed slice thickness should match the collimation and the reconstruction increment and should be <80% of the slice thickness or less. The detailed assessment of small structures, such as peripheral airways in the lung parenchyma, normally requires a high-resolution kernel. However, thin slices together with image reconstruction using a high spatial resolution kernel result in noisy images. The trade-off between high-resolution images—what we are used to when looking at traditional HRCT—and noise represents a major challenge. At the same time the performance of post-processing, segmentation, and quantitation using dedicated software tools is often hampered by noisy high-resolution images, and the use of images reconstructed with a regular soft tissue kernel might be more appropriate (Mayer et al. 2004). Iterative reconstruction is also recommended, although it is presently unclear how quantification by dedicated tools is influenced.

Current studies show the additional potential of reducing the radiation exposure, suggesting that the tube current could even be reduced to 20 mA or less (Dijkstra et al. 2013). This will be so-called ultra-low-dose-CT and is facilitated by new inventions in scanner and post-processing techniques. Additional iterative reconstruction is for sure one of the most auspicious techniques. With an acceptable loss of image quality nowadays it is already possible to reduce the effective radiation dose up to 70% compared with a standard low-dose-CT (Kim et al. 2015).

Technically, the conventional assessment of air trapping is based on a CT acquired in a breath hold after deep expiration (Kauczor et al. 2011). Normally, the removal of air from alveoli will result in an increase of lung tissue density on CT, because a voxel density in Hounsfield Units (HU) is composed of variable combinations of air, lung tissue, and blood. Previous work has shown that the appearance of ground-glass opacities is conserved with low-dose CT, which may be transferred to the

situation of expiratory CT where normal lung tissue will show an increase in density (ground-glass appearance) in expiration compared to the respective anatomical place scanned in inspiration. Thus, low-dose scans with, for example, 20–40 mAs may be used for the acquisition of expiratory scans with modern scanners (Bankier et al. 2007; Kauczor et al. 2011). Such expiratory scans are invariably obtained in conjunction with routine examination obtained at end inspiration in airway diseases.

In addition, significant work has been performed to elucidate the potential role of dynamic CT acquisitions during continuous expiration instead of collecting data at fixed level during expiration only. Such acquisitions require high temporal resolution and are easily performed at a single axial level (Heussel et al. 2001). CT scans acquired during continuous expiration are much more sensitive to diagnose bronchial collapse or air trapping. The improvement by dynamic CT can be explained by the fact that patients have much less difficulty performing an active continuous exhalation instead of maintaining the residual volume after an exhalation for a breath hold period of up to 10 s. However, modern MDCT scanners can also be used to generate volumetric 4D CT data, using a spirometric curve as a signal for retrospective gating. This technology is a translation from ECG-triggered CT scans of the heart to respiratory triggered scans of the lung parenchyma (Ley et al. 2006; Wielpütz et al. 2014).

Datasets acquired with dual-energy scanners and additional i.v. contrast agents allow for the reconstruction of virtual non-enhanced images as well as an iodine distribution image. Color-coded superimpositions of this information will then demonstrate the distribution of iodine as a marker of pulmonary blood volume at a single timepoint. This is a direct representation of the distribution of lung perfusion with a linear relationship between the concentration of iodine and the density measured by CT. Due to the reflex of hypoxic vasoconstriction perfusion defects will match ventilation defects caused by airway disease. As such the functional impairment in airway disease can be assessed by perfusion imaging. The severity can be calculated as the lung volume affected by hypoxic vasoconstriction.

## 2.2 Multiplanar Reformats, MIP, MinIP, and Image Processing

The isotropic datasets allow for different post-processing techniques to be used for evaluation and presentation purposes (Grenier et al. 2003; Fetita et al. 2004). These techniques encompass two-dimensional multiplanar reformats (MPR), which allow to assess the central airways along their anatomical course as well as complex three-dimensional segmentations, and volume rendering, which although a little more time-consuming illustrate the important findings in a very intuitive way, e.g., a frontal view of the patient or a simulation of an intraoperative situs. The perception of the anatomy of the tracheobronchial tree is further enhanced by maximum (MIP) and especially minimal intensity projections (MinIP). These two techniques are helpful in detecting subtle pathologies. MIP images help to characterize pulmonary nodules as peribronchovascular or interlobular just as well as detection of mucoid impaction or tree-in-bud pattern (Bhalla et al. 1996). In contrast, the MinIP images simplify the identification of central airway lumina and define abnormal lung attenuation like ground-glass opacity (Bhalla et al. 1996).

## 2.3 Virtual Bronchoscopy and 3D Views

Nowadays modern volume-rendering techniques (VRT) or SSD (shaded surface display) allow for the visualization of detailed three-dimensional models of the airway tree (Fig. 1). The virtual bronchoscopy uses the SSD technique allowing for a noninvasive intraluminal evaluation of the tracheobronchial tree (De

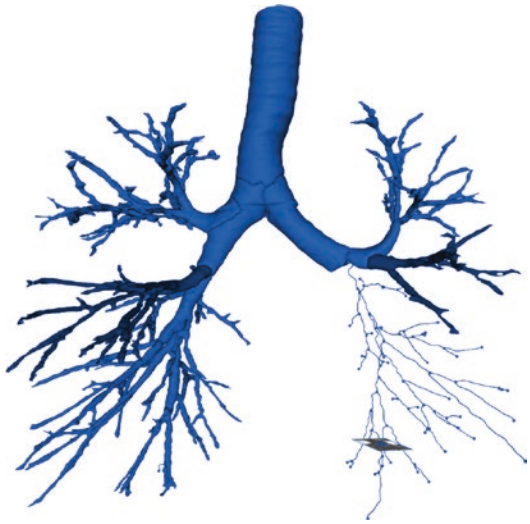

**Fig. 1** 3D volume rendering (VR) after segmentation of the tracheobronchial tree based on a volumetric high-resolution MDCT acquisition of a patient suffering from cystic fibrosis. Prepared with YACTA software, programming by O. Weinheimer, Heidelberg

Wever et al. 2004). New software just requires a seedpoint in the proximal trachea as starting point and a distal goal. The software automatically tracks the way to the target structure. One advantage of virtual bronchoscopy (VB) over classic bronchoscopy is the visualization of the tissue and structures surrounding the airways (e.g., goiter, aorta, or tumor). Therefore, the relationship of a peritracheal lymph node to the trachea or a bronchus can well be displayed for planning a transbronchial needle biopsy. Another advantage over the classic bronchoscopy is in patients with an airway obstruction, caused by tumor or due to external compression. In such situations, it is not possible for the bronchoscopist to pass the stenosis, to see the poststenotic bronchial tree, and to determine the distal extent of the tumor (Kauczor et al. 1996). Performing VB all these answers can be given. With modern MDCT scanners the bronchi down to the seventh or eighth generation can be easily visualized (Reynisson et al. 2015).

## 3 Evaluation

### 3.1 Visual Evaluation

Using grading and scores of elementary features of airway CT like bronchiectasis/bronchiolectasis, bronchial wall thickening, mucus plugging, tree-in-bud pattern, air trapping, or mosaic attenuation pattern help to determine the severity of airway diseases, such as cystic fibrosis, and can be correlated with pulmonary function (de Jong et al. 2004; Brody et al. 2005). This is inherently prone to inter-reader variability, limited reproducibility, and often time-consuming.

### 3.2 Quantitative Evaluation

The dramatically increased acquisition speed, which reduced motion artifacts, as well as the increasing spatial resolution (especially z-axis-resolution) opened the door to the quantitative evaluation of airway dimensions down to subsegmental bronchial level. Volumetric CT allows for the calculation of quantitative indices of bronchial airway morphology, including lumen area, inner and outer diameters, wall thickness, wall area, airway segment lengths, airway taper indices, and airway branching patterns. The complexity and size of the bronchial tree render manual measurement methods impractical and inaccurate (Venkatraman et al. 2006). Airway tree segmentation can be performed manually, which however is tedious and extremely time-consuming (Aykac et al. 2003). On the basis of the volumetric data sets sophisticated post-processing tools will automatically segment the airways down to the 10th or 11th generation (Mayer et al. 2004; Reynisson et al. 2015). This allows for visualization of the tracheobronchial tree without any overlap by surrounding parenchyma as well as for the reproducible and reliable measurements of the segmented airways. The use of curved MPR from MDCT datasets is a solution to measure airway dimensions regardless of their course with respect to the transaxial CT scan.

The simplest segmentation method used a single threshold (cutoff) of pixel values in Hounsfield units (HU). Pixels with HU values lower than the threshold are assigned to the lumen (air), while surrounding pixels with HU values higher than the threshold are assigned to the airway wall or other surrounding tissue. Based on this analysis, the 3D region-growing algorithm extracts all voxels that are definitely airway lumen. However, using a simple global threshold often fails in detecting the wall of smaller airways or is hampered by mucus; thereby such tools often require manual editing. To enhance this basic segmentation process some additional (add-on) algorithms were developed, i.e., based on fuzzy connectivity (Tschirren 2005) or by wave propagation from the border voxels (Mayer et al. 2004). The luminal segmentation result is condensed to the centerline (or skeletonization) running exactly in the center of the airway. These centerline points are the starting points for the airway wall detection and quantification. Approaches include methods based on the estimation of the full width at half-maximum (FWHM), brightness-area product or integral-based method (IBM) (Lo et al. 2012) and pixel-intensity gradient (Reinhardt et al. 1997; Nakano et al. 2005; Berger et al. 2005; Tschirren 2005). In general, by identifying the lumen center through detection of all adjacent voxels with air-density, a centerline can be calculated representing the long axis of each airway. Further, the algorithms measure pixel values along radial rays casting from the lumen center outward beyond the airway wall around 360°. For the FWHM method, for example, the boundary between the lumen and wall is determined by a pixel whose HU value is half the range between the local minimum in the lumen and the local maximum in the airway wall; while the boundary between the wall and lung parenchyma is determined by a pixel whose HU value is half the range between the local maximum in the wall and the local minimum in the parenchyma. Along each radial ray, the inner and outer margins of the airway wall are thus determined, allowing for measurements of the total airway diameter, airway lumen or wall thickness, for example (Weinheimer et al. 2008; Kauczor et al. 2011; Wielpütz et al. 2013b). Further technical developments vary the level of the half density (FWxM) to enable for a measurement of thin airway wall considering the spatial volume effect, etc. (Weinheimer et al. 2008).

## 4 Elementary CT Findings in Airway Diseases

### 4.1 Bronchiectasis and Bronchiolectasis

Throughout the lung, the bronchi and pulmonary arteries run and branch together as a bronchovascular bundle, while pulmonary veins pass separately. The ratio of the size of the bronchus to its adjacent pulmonary artery is widely used as a criterion for detection of abnormal bronchial dilatation. By definition, normal bronchi should have the same inner diameter such as the width of the concomitant pulmonary artery. Bronchiectasis is described as a localized irreversible increase of the bronchial lumen larger than the accompanying vessel. The result of this is the so-called *signet ring sign* (Fig. 11a, b), in which the dilated bronchus is the ring and the nearby artery forms the signet. Bronchiectasis in primary airway disease should be differentiated from traction bronchiectasis caused by lung fibrosis or other entities (Fig. 2). They can occur with

**Fig. 2** Traction bronchiectasis (↗) in a patient with non-specific interstitial pneumonia (NSIP)

or without bronchial wall thickening, mucus-filled dilated bronchi (*flame and blob sign*), plugged and thickened centrilobular bronchioles (*tree-in-bud sign*). The bronchiectasis is morphological categorized in cylindrical (mild bronchial dilatation, regular outline of the airway), varicose (greater bronchial dilatation, accompanied by local constrictions resulting in an irregular outline of the airway) and cystic or saccular (ballooned appearance of the airways, reduced number of bronchial divisions) type (Figs. 4a, 7a, b, 8a and 11). The morphological type is not related to a certain underlying cause.

## 4.2 Bronchial Wall Thickening

Bronchial wall thickening (BWT) is defined as an imaging descriptor of an abnormally thick bronchial wall, which can arise from numerous entities, and is best determined by the T/D-ratio, whereas T represents the wall thickness and D the overall bronchial diameter (Little et al. 2002) (Figs. 7a, 8a, and 9a, b). Normal is a ratio smaller than 0.2 (Webb et al. 2001). In the future, a more objective quantification of BWT should be established.

## 4.3 Mucus Plugging

Mucus plugging or mucoid impaction describes an airway filled by mucoid secretions. A variety of congenital and acquired abnormalities can cause mucoid impaction, most common with segmental bronchial atresia, disorder of mucociliar clearance, immunodeficiencies, and cystic fibrosis as an example for congenital entities or with acquired allergic bronchopulmonary aspergillosis. Mucoid impaction can occur together with bronchiectasis, which is called bronchocele resulting in the *finger-in-glove sign*, whereat the mucus is plugged in the large debranching airways (Martinez et al. 2008).

## 4.4 Tree-in-Bud Pattern

The tree-in-bud pattern represents an appearance of multiple centrilobular micronodules connected to branching linear structures originating from a single stalk that resembles a budding tree (Fig. 3a, b). These nodules correspond to the very distal airways, e.g., the terminal bronchioles. Because CT resolution precludes the depiction of normal small airways smaller than 2 mm approximately, a tree-in-bud pattern and thus visibility of such

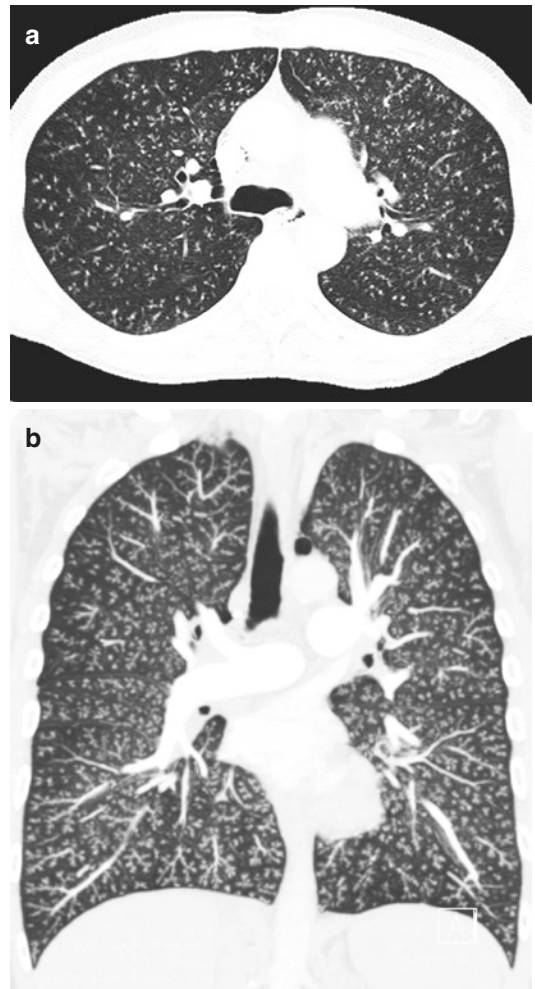


**Fig. 3** (**a**, **b**) 10 mm MIP in axial (**a**) and coronal (**b**) plane of MDCT with widespread *tree-in-bud pattern* in a patient with bronchiolitis, which consists of multiple centrilobular micronodules connected to linear structures originating from a single stalk that resembles a budding tree. Note the subpleural sparing where no airways are present

small airways reflects a pathologic increase in size through wall thickening, dilatation or mucus filling, or a combination of these. Like the other elementary CT findings, it is recognized in a large number of pulmonary abnormalities, including peripheral airway diseases such as infection (bacterial, viral, or fungal), congenital entities (cystic fibrosis, primary ciliary dyskinesia), aspiration, inhalation, or immunologic disorders (Rossi et al. 2005). Usually MIP reconstructions help to clearly identify this pattern and to differentiate it against a random pattern, for example.

## 4.5 Mosaic Attenuation Pattern and Air Trapping

Mosaic attenuation pattern is characterized by heterogeneous attenuation of the lung parenchyma with areas of hypoattenuation and ground-glass attenuation side-by-side, often but not necessarily delineated sharply by secondary lobules or whole lobes (Ridge et al. 2011). This phenomenon may be caused by inflammation, vascular disorders, or obstructive airway disease, sometimes interconnected (Stern et al. 1995). In case of (small) airway obstruction, which prevents the air from being exhaled, a reduced alveolar oxygen level and hyperinflation induces the physiological mechanism of hypoxic pulmonary vasoconstriction, or formerly "Euler-Liljestrand reflex." It downregulates the perfusion of non-ventilated/hypoxic lung areas in order to avoid intrapulmonary shunting (Euler and Liljestrand 1946; Wielpütz et al. 2016). These two mechanisms, localized hyperinflation and co-localized perfusion reduction, lead to a hyperlucency of the affected area on CT. Importantly, this area also presents with a rarefication of the vasculature with respect to number and size of visible vessels.

In order to differentiate mosaic attenuation due to airway obstruction from other causes (vascular, inflammatory, interstitial lung disease), additional expiratory CT is recommended (Miller et al. 2014). Pulmonary function tests (for example, FEV1, the forced expiratory volume in 1 s) can be insensitive to the detection of small airway disease, and imaging may be the key diagnostic test. Due to the limited resolution of CT, a voxel of the lung contains variable compositions of air, lung tissue, and blood. In any case where the air-content is reduced relative to the other components, the density in HU will subsequently increase. As long as some air is retained, larger areas of these voxels will present as ground-glass attenuation/opacity, where the underlying tissue and vessel texture will be preserved, as opposed to consolidation, whereat those structures are obscured.

By performing expiratory CT, air is removed from healthy lung areas, thus the density of these regions increases. As described above, in case of an airway disease with obstruction especially of the small airways, the air is captured and cannot be exhaled. Accordingly, no or minor change in tissue density in the comparison between inspiratory and expiratory CT can be appreciated (usually <50 HU change). Such areas can then be identified as "*air trapping,*" a terminology used for the appearance of mosaic attenuation in the context of expiratory CT (Fig. 4a–d). Air trapping is often seen in patients with chronic obstructive pulmonary disease (COPD), bronchiolitis obliterans (BO) (see Sect. 5.14) or cystic fibrosis (see Sect. 5.6). If these hyperlucent areas increase in density after expiration, it is assumed that the underlying disease has a vascular origin, e.g., pulmonary hypertension, pulmonary embolism.

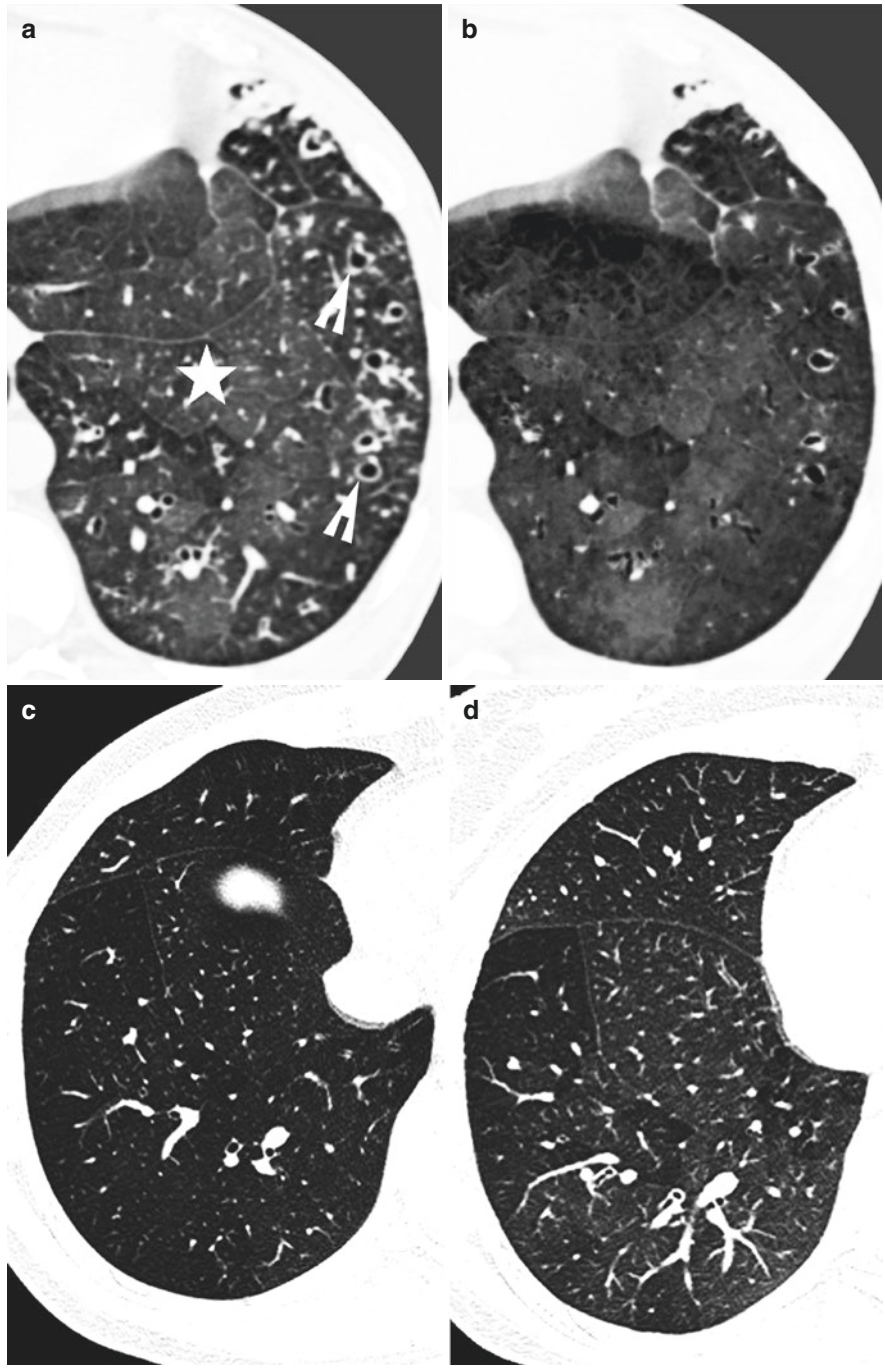


**Fig. 4** (**a**–**d**) Patient with severe peripheral destructive bronchiectasis (➶) and *mosaic attenuation* (★) sharply delineated corresponding to secondary lobules. (**a**) 1 mm axial reconstruction; (**b**) MinIP reconstruction (5/1 mm), which is very helpful to identify *mosaic attenuation.* Inspiratory CT of another patient (**c**) with mild hyperlucent areas of the lateral and dorsal right lower lobe and reduction of vasculature with respect to number and size of visible vessels. Expiratory scan of the same patient (**d**) with a lack of an increase of attenuation or volume reduction in contrast to the healthy lung. These findings are consistent with *air trapping*

## 5 Diseases

### 5.1 Tracheobronchomalacia

A common indication for imaging of the trachea is suspected tracheobronchomalacia (TBM). It has to be differentiated from tracheal stenosis, which is a nonfunctional luminal narrowing of the airway, frequently of short length (i.e., few cm) and causes only limited respiratory impairment. Both diseases might appear in combination. The definition of TBM used by many authors in the radiological as well as in the bronchoscopic community refers to a significant tracheal instability in case of a >50% decrease of the cross-sectional area (CSA) of the trachea during forced expiration (Loring et al. 2007) (Fig. 5a, b). Excessive expiratory collapse of the trachea can be caused by two pathological mechanisms: either by weakness of the supporting airway cartilage or by an excessive invagination of the posterior membraneous segment of the trachea. An in-depth review shows that these are two distinct clinicopathological entities, which may or may not coincide. Following this review only excessive collapsibility involving weakness of airway cartilage should be addressed as TBM, whereas the term excessive dynamic airway collapse (EDAC) should be used in case of excessive invagination of the posterior wall of the trachea without signs of cartilaginous involvement (Murgu and Colt 2006). However, most of the published work in the radiological literature does not separate these two mechanisms and mostly uses the term TBM for both mechanisms leading to an expiratory collapse of the trachea.

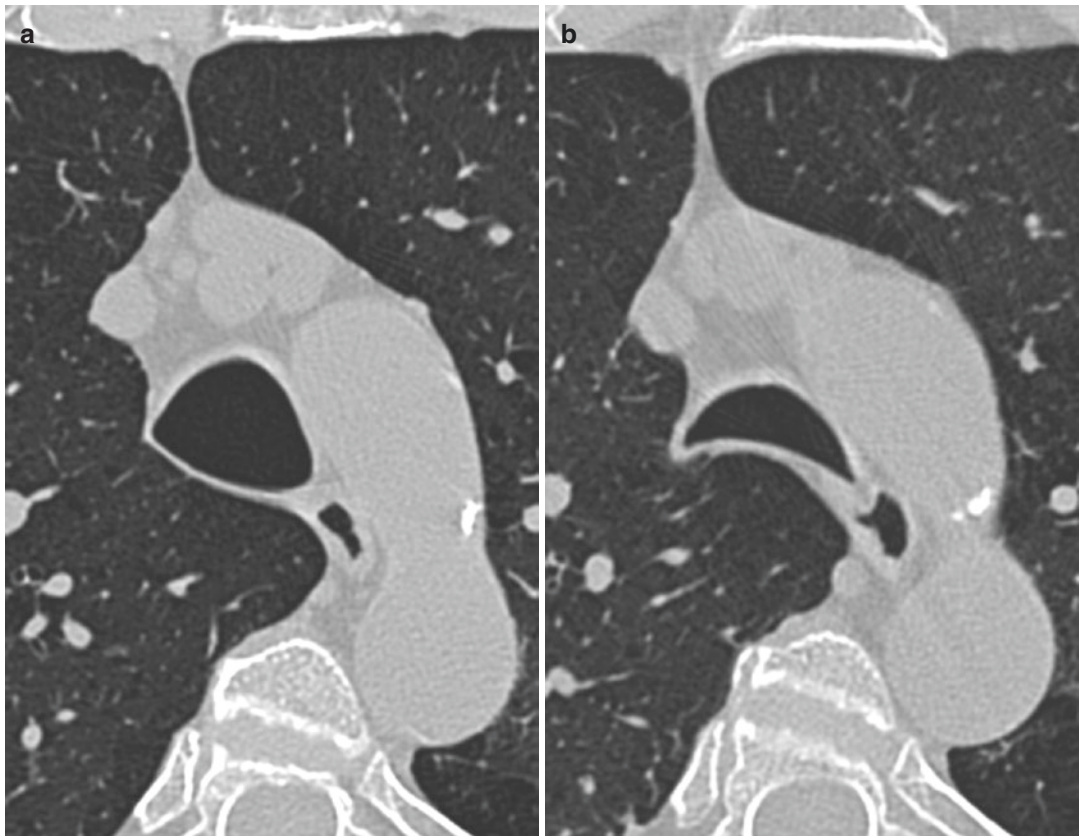


**Fig. 5** (**a**, **b**) Moderate expiratory collapse of the trachea in a patient with advanced COPD (**a**) at suspended full inspiration, and (**b**) cine CT during shallow respiration, expiratory phase shown. This finding is consistent with crescent-type tracheobronchomalacia

Conditions leading to acquired TBM/EDAC include COPD, tracheal tumor, tracheitis, relapsing polychondritis as well as a history of prolonged intubation, tracheotomy or prior radiotherapy (Carden et al. 2005).

The acquired form of excessive expiratory collapse is to be considered as one of common causes of chronic cough, expiratory dyspnea, and recurrent respiratory infections. Since these symptoms are highly unspecific and TBM/EDAC escapes detection on routine clinical and imaging investigations it is considered a highly underdiagnosed condition. The prevalence varies from 23% in patients with chronic bronchitis (Jokinen et al. 1976) over 10% in patients referred for the evaluation of pulmonary embolism (Hasegawa et al. 2003) to 4.5% in a large retrospectively reviewed bronchoscopic series (Jokinen et al. 1977) and is the most common congenital anomaly of the central airways (Holinger 1980).

Since the pathology involves the dynamic process of expiration TBM/EDAC cannot be sufficiently depicted by static end-inspiratory or end-expiratory CT scans alone. A paired inspiratory/expiratory investigation is the absolute minimum diagnostic approach (Hein et al. 2000; Boiselle et al. 2003). Dynamic examination protocols have been shown to be clearly superior over breath-hold acquisitions for the determination of TBM (Heussel et al. 2001; Baroni et al. 2005). Dynamic imaging also resulted in a significant number of changes of therapy.

At least, two different protocols have been proposed. The first one includes a dynamic expiratory spiral scan (20–40 mAs, 0.5 s gantry rotation time, 80–120 kVp, 1–2.5 mm collimation, pitch equivalent of 1.5) during a forced expiration maneuver (Baroni et al. 2005). This scan covers the trachea and the main bronchi in the region between the low cervical region and the level 2 cm below the carina and is acquired in the craniocaudal direction. Due to a naturally given high contrast between airway lumen and wall, low dose techniques can be used without compromising the assessment of suspected TBM/EDAC (Zhang et al. 2003). The examination protocol proposed by Heussel et al. includes a temporally resolved scan (no table feed, "cine CT"; no interscan delay, reconstruction interval 100 ms) over the region of suspected TBM/EDAC in shallow respiration (Heussel et al. 2001). This work published in 2001 was performed on a 4-slice CT with consecutively small spatial coverage. Modern 64 slice CT offer the possibility of simultaneous imaging a region with a craniocaudal extension of 3 cm with the same scan technique (Boiselle et al. 2006), depending on detector size.

The evaluation is twofold: (1) evaluation of the degree of collapse; and (2) analysis of the shape change of the trachea. For this purpose, the dynamically acquired images are compared to those acquired at suspended end-inspiration. The degree of collapse can be evaluated visually or better by calculating the change of the CSA with manual or semi-automatic segmentation tools for the tracheal lumen. Using the same diagnostic criterion for TBM/EDAC as bronchoscopy (greater than 50% reduction in CSA of the airway lumen at expiration) CT was shown to have at least similar accuracy when compared to invasive bronchoscopy (Gilkeson et al. 2001; Zhang et al. 2003; Sun et al. 2007). The reduction of the tracheal lumen is associated with an obvious change of the shape, which can be oval or crescentic. The crescentic form (*frown sign*) is due to the inward bowing of posterior membrane of the trachea (Boiselle et al. 2006). Concerning the therapeutic relevance of diagnosing TBM/EDAC a short-term follow-up study of patients with severe TBM/EDAC undergoing central airway stabilization with silicone stents concluded that the intervention markedly improved dyspnea, health-related quality of life, and functional status in these patients (Ernst et al. 2007).

## 5.2 Tracheobronchomegaly (Mounier-Kuhn Syndrome)

The Mounier-Kuhn syndrome is a rare disease, which shows an obvious dilatation of the trachea and main-stem bronchi with a peak in the fourth or fifth decade of men (Kwong et al. 1992). It is associated with atrophy of cartilaginous, muscular,

and elastic components of the tracheal wall, and may be often seen in a variety of mostly congenital systemic diseases resulting in connective tissue abnormalities, e.g., Ehlers-Danlos or Marfan syndrome (Shin et al. 1988). CT findings include a thinning of the tracheal wall (normal wall thickness 1–3 mm) and a dilated tracheal diameter of more than 2.1 cm for women, respectively 2.5 cm for men (Woodring et al. 1991) (Fig. 6).

## 5.3 Tracheal Stenosis

Mostly fixed, as opposed to dynamic TBM/EDAC, tracheal stenoses are a complication of long-term tracheal intubation. Narrowing may occur at the stoma site after tracheostomy, at the level of the inflatable cuff, or, less commonly, where the tip of the tube has impinged on the tracheal mucosa (Stark 1995).

Further causes of airway narrowing are neoplastic lesions. They can exhibit a predilection for the one of the three compartments: lumen, wall, or surrounding soft tissue. For the trachea 90% of the primary tumors in adults are malignant, mainly squamous cell carcinoma (55%) or adenoid cystic carcinoma (18–40%). Only 10% are benign neoplasms such as papilloma, true mucinous adenoma, hamartoma, fibroma, chondroma, leiomyoma, and granular cell myoblastoma. In the bronchi non-small cell lung cancer prevails (Marom et al. 2001).

External compression of the mediastinal airways may occur due to enlarged lymph nodes/metastasis or other mediastinal structures (e.g., thyroid goiter, aortic aneurysm, vessel anomalies, such as a double aortic arch or pulmonary artery sling) or tumors (e.g., teratoma or thymoma). Intrapulmonary bronchial carcinoma or other tumors of more peripheral airways may also act as external compressors.

**Fig. 6** Inverted coronary thick-slice MinIP of a patient with tracheobronchomegaly (Mounier-Kuhn syndrome)

## 5.4 Saber Sheath Trachea

Saber sheath trachea is a tracheal pathology in COPD patients with a substantially decreased coronal diameter of the trachea, which is different from the excessive collapsibility of the trachea during expiration, which may also be encountered in COPD patients. It is defined as an intrathoracic narrowing of the trachea, with the coronal diameter equal to or less than two-thirds of the sagittal diameter, when measured 1.0 cm above the top of the aortic arch (Trigaux et al. 1994). The saber sheath trachea by itself does not have a clinical significance, rather due to the highly significant correlation with COPD (>95%) (Trigaux et al. 1994).

## 5.5 Primary Ciliary Dyskinesia (Immotile Cilia Syndrome)

The primary ciliary dyskinesia—also known as immotile cilia syndrome—is a congenital and inherited defect of the hair-like motile cilia of the epithelial layer of the airways. Usually they are responsible for cleaning the airways by clearing mucus, debris, and bacteria by coordinated beating (Lucas et al. 2014). The prevalence shows a large variation between 1:2,200 and 1:40,000 (Kuehni et al. 2010). The diagnosis is often missed or prolonged and in general made at the age of 4.5–6.8 years (Kuehni et al. 2010). The defect does not only affect the airways but also

the sinuses and the ear. Immediately after birth the neonates present with rhinitis or an obstructed nose resulting in feeding problems (Werner et al. 2015). Affected children complain of chronic sinusitis, otitis media, cough, and recurrent upper or lower airway infections. In 40–50% it is combined with a situs inversus, which is easily appreciated and then called *Kartagener's syndrome*. The most striking findings at CT are bronchiectasis, predominantly in the middle and lower lobe, whereas the severity correlates with older age and worse pulmonary function (Kennedy et al. 2007), and bronchial wall thickening (Fig. 7a, b). Nine percent of the patients present with a pectus excavatum (Kennedy et al. 2007).

## 5.6 Cystic Fibrosis

Cystic Fibrosis (CF) or mucoviscidosis is an autosomal recessive disorder caused by mutations of the CFTR-gene (Cystic Fibrosis Transmembrane Regulator-Protein), which functions as a Cl-channel of the cell. The impaired CFTR function causes aberrations of volume and ion composition of airway surface fluid, leading to viscous secretions with the consequence of bacterial colonization, chronic lung infection, airway obstruction and consecutive destruction of the lung parenchyma and airways (Puderbach et al. 2007b) (Fig. 8a, b). Despite improved understanding of the underlying pathophysiology and introduction of new therapies, CF is still the


**Fig. 7** (**a**) Patient with *Kartagener's syndrome* presenting with a situs inversus, cylindrical bronchiectasis (➶) and bronchial wall thickening, predominantly in the lower lobe. (**b**) Patient with *primary ciliary dyskinesia* presenting with hyperlucency of the right middle lobe (★) as well as cylindrical to cystic bronchiectases of the left upper lobe (➶)

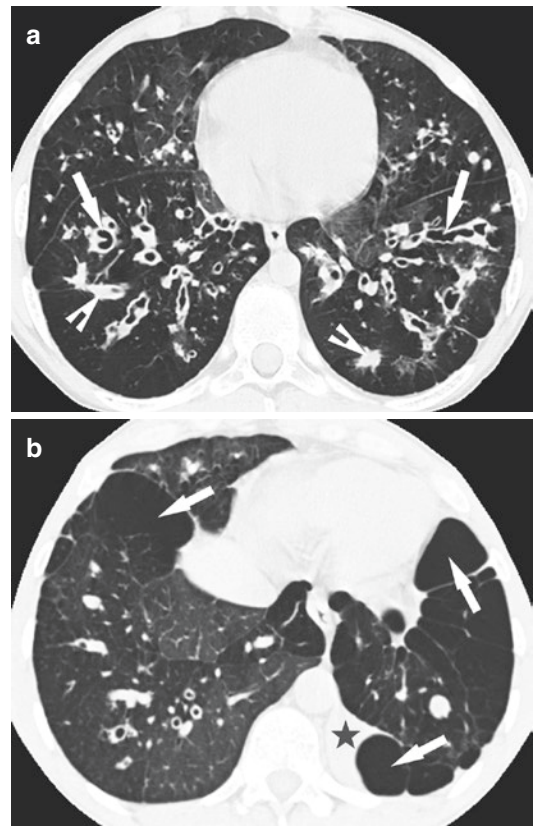


**Fig. 8** (**a**) *Cystic fibrosis (*CF*)* patient showing varicose bronchiectasis with bronchial wall thickening (➶) and mucus plugging (➶) as well as mosaic attenuation on inspiratory CT. (**b**) Another patient with typical findings of CF including mosaic attenuation, and additional lung emphysema (➶) and atelectatic left lower lobe (★)

most frequent life-shortening inherited disease in the white population. Advantages in knowledge and medical care resulted in a dramatic increase of the life span for these patients. The median of survival in CF patients in Germany is >40 years still with an upward trend (Dodge et al. 2007). CF affects most body systems, but the majority of morbidity and mortality in CF patients is due to lung disease, and thus repeated imaging of the chest is required. The standard radiological tools for imaging of the chest has been chest-X-ray and CT. CT has been shown to be more sensitive to early CF lung disease than pulmonary function testing, likely due to the regional nature of the information obtained. The structural changes of CF lung disease include bronchial wall thickening, mucus plugging, bronchiectasis, air fluid levels, consolidation, and segmental/lobar destruction (Puderbach et al. 2007a). The better sensitivity of CT in the detection of lung damage beyond that of chest radiography has long been recognized (Bhalla et al. 1991; Maffessanti et al. 1996). Nowadays the CT scanning protocol should include inspiratory and expiratory scans to enhance the sensitivity for small airway obstruction due to the possibility to detect air trapping (Wielpütz et al. 2016).

Scoring systems for thin-section CT have frequently been used to quantify airway abnormalities (Bhalla et al. 1991; Helbich et al. 1999; de Jong et al. 2004). All of these scoring systems rely on composite scores to semiquantitatively estimate features on CT scans. However, this approach was limited to patients with mild lung disease in whom the FEV1 value usually is normal despite the presence of abnormal airways and an exaggerated inflammatory response (Khan et al. 1995; Tiddens 2002). It was reported that the scoring systems for thin-section CT might be more sensitive than the PFT (Pulmonary function testing) in the detection of disease progression (de Jong et al. 2004).

Because of the rising life expectancy of these patients and the repetitive need for follow-up chest imaging the aspect of cumulative radiation dose becomes more and more important. So the improving MRI technologies of chest imaging will play a major role in future as MRI has the ability to be used as an appropriate alternative (Puderbach et al. 2007b) with the potential of acquisition of additional information by performing functional chest imaging, e.g., lung perfusion and ventilation (Wielpütz et al. 2013a).

Quantification of the structure of the lung includes evaluation of the parenchyma and the airway walls. The large airway wall abnormalities can be assessed by airway wall measurement, and small airway and parenchymal abnormalities can be assessed by changes in lung parenchymal attenuation or air trapping (Brody et al. 2005). The first quantitative airway analysis was performed on thin section CT images. Thicker walls and dilated airways were reported for infants and young children with CF when compared to normal infants (Long et al. 2004). The ratio between airway lumen area and the area of the accompanying pulmonary artery as well as between airway wall area and the area of the accompanying pulmonary artery was increased, and the airway walls were thickened (de Jong et al. 2005). Although lung function did not change significantly over a 2-year follow-up period, there were significant changes in quantitative airway wall thickening (de Jong et al. 2005). Due to technical limitations of thin section CT as pointed out above, the acquisition of volumetric datasets with subsequent quantification in 3D obviously makes sense. Total diameter, lumen area, and wall thickness can be assessed with dedicated software tools and are valuable indexes for determining the severity of airway disease in patients with CF (Montaudon et al. 2007; Wielpütz et al. 2013a).

### 5.7 Tracheobronchial Amyloidosis

The tracheobronchial amyloidosis (TA) is the most common subtype of thoracic amyloidosis (Chung et al. 2011). CT shows tracheal surface irregularities, focal circumferential wall thickening, and widespread dense mural calcifications typically concentrically as well (Fig. 9a, b), whereas the tracheobronchopathia osteochondroplastica and relapsing polychondritis spare the posterior wall (O'Regan et al. 2000).

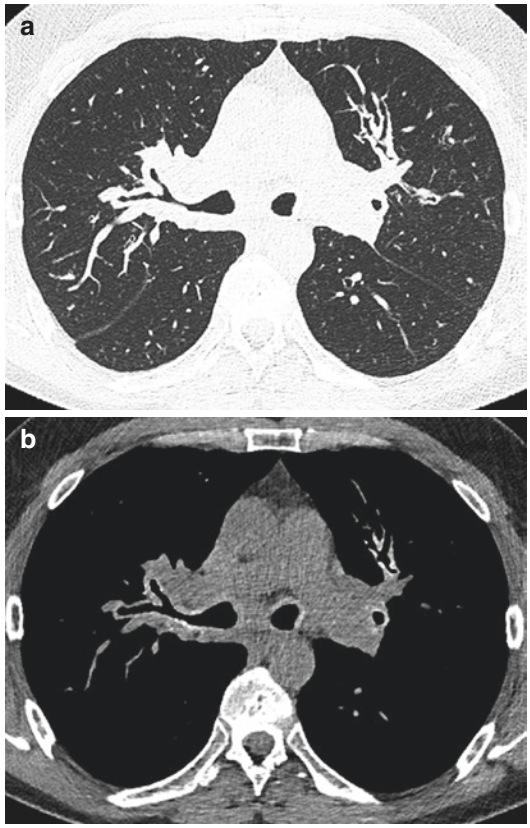


**Fig. 9** *Tracheobronchial amyloidosis* with extensive circumferential wall thickening and peripheral surface irregularities in the lung window (**a**) and mural calcifications in the soft tissue window (**b**)

## 5.8 Sarcoidosis of the Airways

Sarcoidosis is a multisystem chronic inflammatory disorder of unknown etiology characterized by non-caseous epithelioid cell granulomas and changes in tissue architecture, affecting almost any organ (Criado et al. 2010). Involvement of the lung is seen in over 90% of patients. The airways are affected in 65% of patients showing wall thickening, luminal narrowing, or stenosis. Traction bronchiectasis and air trapping with mosaic attenuation pattern can be seen as well. Due to hilar and mediastinal lymphadenopathy a secondary tracheal narrowing is often present. The characteristic epithelioid cell granulomas not only affect the lung itself but also the tracheal wall, resulting in primary tracheal stenosis.

## 5.9 Relapsing Polychondritis

Relapsing polychondritis (RP) is a multisystem inflammatory disease affecting the cartilage and tissues rich in proteoglycan. The RP is characterized by recurrent inflammatory episodes affecting the cartilage in various locations. The prevalence is approximately 3.5:1,000,000 with a peak in the fifth decade (Trentham and Le 1998; Letko et al. 2002). Because of the affection of cartilaginous tissue patients suffer from arthritis with joint pains, saddle nose deformity or cauliflower ears. In case of a laryngotracheal involvement early symptoms are pain and tenderness over the thyroid cartilage and trachea followed by cough, hoarseness, stridor, wheezing, or dyspnea (Sharma et al. 2013). In up to 50% the airways are affected (Trentham and Le 1998) resulting in a loss of stability of the trachea and bronchi, which are kept open by cartilaginous rings and structures. MDCT can demonstrate the classic morphologic airway changes associated with RP, including fixed airway narrowing and wall thickening (Lee et al. 2006). A wall thickening of the anterior and lateral tracheal wall with marked sparing of the posterior wall—corresponding to the horseshoe-shaped tracheal cartilage—are pathognomonic for RP (Fig. 10a, b). It is mandatory to perform dynamic CT scanning protocols including end-inspiratory and dynamic expiratory imaging alternatively. Air trapping and airway calcification are very common as well (Lee et al. 2006).

## 5.10 Granulomatosis with Polyangiitis

Granulomatosis with polyangiitis (GPA), previously known as "Wegener's granulomatosis" is an inflammatory disease, characterized by a necrotizing vasculitis of the small and medium-sized vessels of the upper and lower airways and glomerulonephritis. Less often there is an involvement of the large joints and the central or peripheral nervous system. The pathomechanism hasn't been investigated yet, but an autoimmune component is suggested, because of the presence

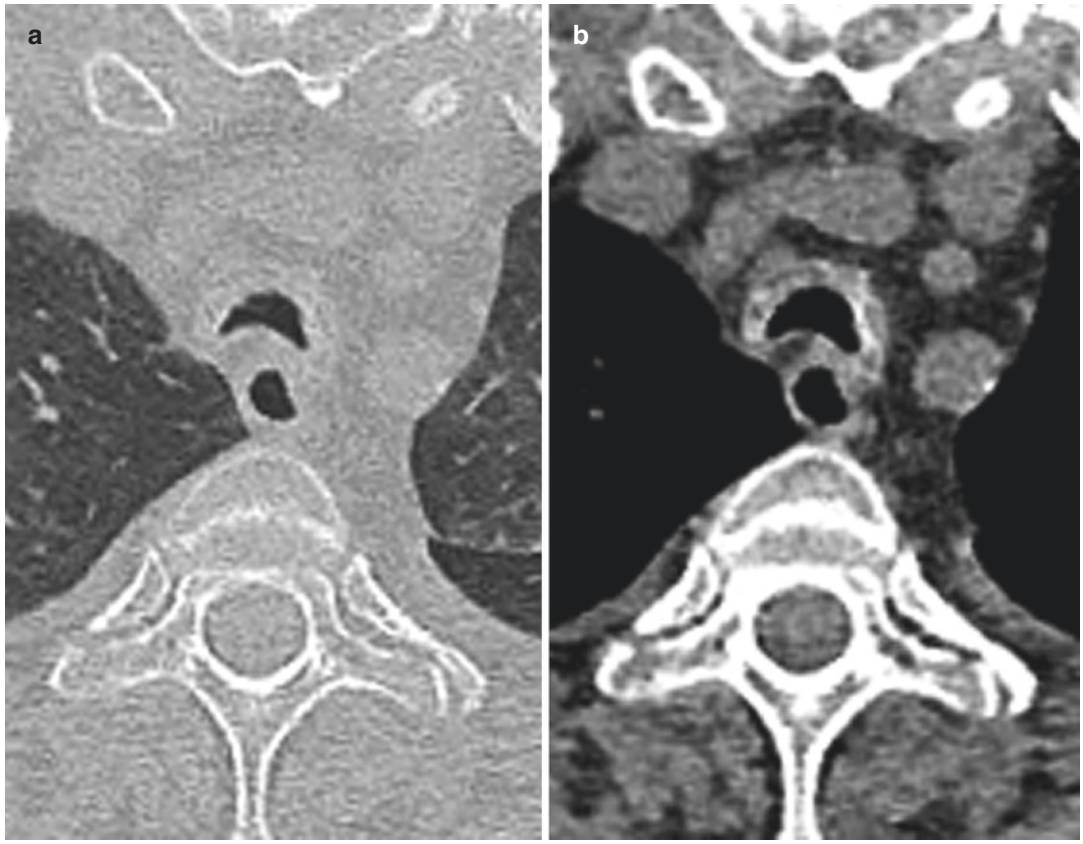


**Fig. 10** (**a**) Lung window and (**b**) soft tissue window of a patient with relapsing polychondritis showing thickening of the anterior and lateral tracheal wall corresponding to the horseshoe-shaped tracheal cartilage, but marked sparing of the posterior membrane

of antineutrophil cytoplasmic antibodies (ANCAs) (Borgmann and Haubitz 2004). The prevalence is about 3.5:100,000 and can occur at any age with a peak between 45 and 60 years (Comarmond and Cacoub 2014). The typical clinical presentation caused by affection of the upper airways is sinusitis, nasal mucosa ulcers, subglottic stenosis, hoarseness, stridor, and dyspnea. If the lower airways are involved patients suffer from cough, hemoptysis, or chest pain. In CT solitary or multiple pulmonary nodules or masses ranging from a few mm to 10 cm with a random distribution can be observed (Martinez et al. 2012). Central cavitation is present in up to 50% in lesions >2 cm (Maskell et al. 1993). Cavitation walls can be smooth and thin or irregular and thick with or without a *halo sign*, originated by surrounding ground-glass opacity. Additionally in about 50% there are ground-glass opacities with a variable distribution, most often peribronchovascular or perihilar, size or density (Sheehan et al. 2003). In case of consolidation they may exhibit positive bronchograms. In a quarter there is an involvement of the trachea, most frequently of the subglottic portion with a circumferential thickening of the tracheal wall, which helps in the differentiation of RP (sparing of the posterior wall) (Martinez et al. 2012). Tracheal stenosis, typically of the subglottic portion will be the result of an inadequate therapy. Affection of the lower airways will cause bronchial wall thickening and bronchiectasis. Typically, there is also an involvement of the upper airways and the paranasal sinuses (Marković et al. 2016; Nakamaru et al. 2016; Eren et al. 2017).

## 5.11 Tracheopathia Osteoplastica

The tracheopathia osteoplastica (TO) or tracheobronchopathia osteochondroplastica is a very rare idiopathic entity elicited by multiple submucosal osteocartilaginous nodules and growth along the anterior-lateral trachea with a distribution along the cartilaginous rings (Meyer and White 1998). TO can occur in almost every age with a peak in the fifth decade. The pathognomonic findings in chest CT are the presence of calcified nodules protruding in the tracheal lumen resulting, if very distinctly, in tracheal stenosis. The posterior wall is always spared. In most cases a long segment of the trachea is affected but sometimes extend to the lobar or segmental bronchi (Hussain and Gilbert 2003). It has to be differentiated from calcifications of the bronchial cartilage, which occur frequently at older age without protruding into the airway lumen. Overall TO is a benign, slowly progressing disorder.

## 5.12 Asthma

Asthma already affects 10% of the world population and is still on the rise. Chronic inflammation in patients with asthma leads to airway remodeling (Kauczor et al. 2011). Typical CT findings are bronchial wall thickening, narrowing of segmental airways, areas of decreased lung attenuation, air trapping, bronchiectasis, and sometimes emphysema (Aysola et al. 2010). Several studies showed a correlation between the dimension of airway changes and the degree of airway obstruction (Donohue et al. 2013). Airway wall thickening may be partially reversible with mid-term inhaled corticosteroid treatment in steroid-naive patients (Niimi et al. 2004). Thus, CT of asthma patients may appear completely normal. However, segmental parenchymal perfusion defects may occur in the respective imaging.

## 5.13 Bronchiolitis

Bronchiolitis is a very broad term, which belongs to an infectious or noninfectious inflammation of the bronchioles. The infectious type is often caused by viruses (in virologically confirmed cases >70% due to respiratory syncytial viruses) (Papadopoulos et al. 2002). Many other causes are possible. The patients are typically young, mostly in the first 2 years, and complain about cough and chronic or progressive breathlessness. Typical CT findings are multiple centrilobular nodules, usually associated with tree-in-bud pattern (Gruden and Webb 1993) (Fig. 3a, b). Bronchial wall thickening is often present as well. In some cases ground-glass opacities or consolidations are found. In an additional expiratory scan air trapping can be visible.

## 5.14 Bronchiolitis Obliterans

Bronchiolitis obliterans (BO) or also known as obliterative bronchiolitis is a special type of the nonspecific inflammatory bronchiolitis with submucosal and peribronchial fibrosis resulting in obstruction and stenosis of the membranous and respiratory bronchioles. BO can be idiopathic or associated with connective tissue diseases, inhalation of toxins, drugs, and chronic graft-versus-host disease (GVHD) (Afessa et al. 2001). Typically, diffuse inflammation of the lung parenchyma is absent. Clinical presentation is the result of the limitation of airflow like dry cough, dyspnea, and wheezing. Air trapping, bronchial dilatation, bronchiolectasis, or hypoattenuation are very common (Fig. 11a-c). To differentiate air trapping expiratory CT scans are necessary, especially in cases in which only the small airways are diseased without visible affection of larger airways. Additional spirometric tests for the quantification of obstruction and also arterial blood gas measurements should be performed.

## 5.15 Swyer-James Syndrome

The Swyer-James syndrome (SJS) is a rare lung condition as a form of postinfectious bronchiolitis obliterans with lucency of the unilateral hemithorax (Fig. 12). It typically follows a viral respiratory infection in infancy or childhood

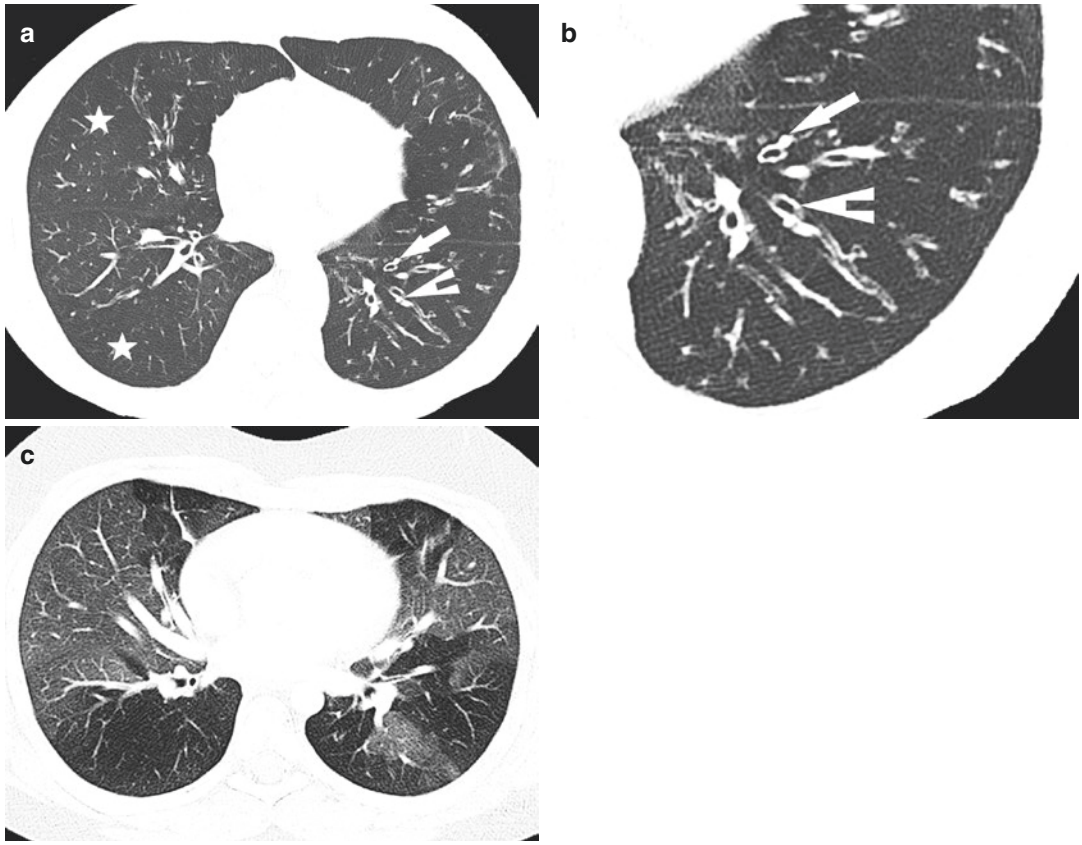


**Fig. 11** (**a**) Patient with *bronchiolitis obliterans (BO)* due to drug toxicity. (**b**) Magnified image of the left lower lobe showing affection of the larger airways with cylindric bronchiectasis (➶), bronchial wall thickening and absence of inflammatory affection of the lung parenchyma. Mosaic attenuation and reduced vasculature are present (★). Also note the *signet ring sign* (➶). (**c**) Another patient with *BO* presenting with almost exclusively bipulmonary mosaic attenuation without visible affection of the large airways

**Fig. 12** *Swyer-James syndrome* with hyperlucency, hyperinflation and rarefication of vessels in the left lung

(Daniel et al. 1984), e.g., adenoviruses or mycoplasma pneumonia infections. The lobes of the affected lung are typically smaller, show a decreased vascularity, hyperinflation, and often bronchiectasis.

## References

Afessa B, Litzow M, Tefferi A (2001) Bronchiolitis obliterans and other late onset non-infectious pulmonary complications in hematopoietic stem cell transplantation. Bone Marrow Transplant 28:425–434

Aykac D, Hoffman EA, McLennan G, Reinhardt JM (2003) Segmentation and analysis of the human airway tree from three-dimensional X-ray CT images. IEEE Trans Med Imaging 22:940–950

Aysola R, de Lange EE, Castro M, Altes TA (2010) Demonstration of the heterogeneous distribution of asthma in the lungs using CT and hyperpolarized helium-3 MRI. J Magn Reson Imaging 32:1379–1387

Bankier AA, Schaefer-Prokop C, De Maertelaer V et al (2007) Air trapping: comparison of standard-dose and simulated low-dose thin-section CT techniques. Radiology 242:898–906

Baroni RH, Feller-Kopman D, Nishino M et al (2005) Tracheobronchomalacia: comparison between end-expiratory and dynamic expiratory CT for evaluation of central airway collapse. Radiology 235:635–641

Berger P, Perot V, Desbarats P et al (2005) Airway wall thickness in cigarette smokers: quantitative thin-section CT assessment. Radiology 235:1055–1064

Bhalla M, Naidich DP, McGuinness G et al (1996) Diffuse lung disease: assessment with helical CT—preliminary observations of the role of maximum and minimum intensity projection images. Radiology 200:341–347

Bhalla M, Turcios N, Aponte V et al (1991) Cystic fibrosis: scoring system with thin-section CT. Radiology 179:783–788

Boiselle PM, Feller-Kopman D, Ashiku S et al (2003) Tracheobronchomalacia: evolving role of dynamic multislice helical CT. Radiol Clin N Am 41:627–636

Boiselle PM, Lee KS, Lin S, Raptopoulos V (2006) Cine CT during coughing for assessment of tracheomalacia: preliminary experience with 64-MDCT. Am J Roentgenol 187:W175–W177

Borgmann S, Haubitz M (2004) Genetic impact of pathogenesis and prognosis of ANCA-associated vasculitides. Clin Exp Rheumatol 22:S79–S86

Brody AS, Tiddens HAWM, Castile RG et al (2005) Computed tomography in the evaluation of cystic fibrosis lung disease. Am J Respir Crit Care Med 172:1246–1252

Burgel PR, Bergeron A, de Blic J et al (2013) Small airways diseases, excluding asthma and COPD: an overview. Eur Respir Rev 22:131–147

Carden K, Boiselle P, Waltz D, Ernst A (2005) Tracheomalacia and tracheobronchomalacia in children and adults: an in-depth review. Chest 127:984–1005

Chung JH, Kanne JP, Gilman MD (2011) CT of diffuse tracheal diseases. Am J Roentgenol 196:W240–W246

Comarmond C, Cacoub P (2014) Granulomatosis with polyangiitis (Wegener): clinical aspects and treatment. Autoimmun Rev 13:1121–1125

Criado E, Sánchez M, Ramírez J et al (2010) Pulmonary sarcoidosis: typical and atypical manifestations at high-resolution CT with pathologic correlation. Radiographics 30:1567–1586

Daniel TL, Woodring JH, Vandiviere HM, Wilson HD (1984) Swyer-James syndrome—unilateral hyperlucent lung syndrome. A case report and review. Clin Pediatr (Phila) 23:393–397

de Jong PA, Nakano Y, Hop WC et al (2005) Changes in airway dimensions on computed tomography scans of children with cystic fibrosis. Am J Respir Crit Care Med 172:218–224

de Jong PA, Ottink MD, Robben SGF et al (2004) Pulmonary disease assessment in cystic fibrosis: comparison of CT scoring systems and value of bronchial and arterial dimension measurements. Radiology 231:434–439

De Wever W, Vandecaveye V, Lanciotti S, Verschakelen JA (2004) Multidetector CT -generated virtual bronchoscopy: an illustrated review of the potential clinical indications. Eur Respir J 23:776–782

Dijkstra AE, Postma DS, ten Hacken N et al (2013) Low-dose CT measurements of airway dimensions and emphysema associated with airflow limitation in heavy smokers: a cross sectional study. Respir Res 14:11

Dodge JA, Lewis PA, Stanton M, Wilsher J (2007) Cystic fibrosis mortality and survival in the UK: 1947–2003. Eur Respir J 29:522–526

Donohue KM, Hoffman EA, Baumhauer H et al (2013) Asthma and lung structure on computed tomography: the Multi-Ethnic Study of Atherosclerosis Lung Study. J Allergy Clin Immunol 131:361–368.e11

Eren E, Kalkan T, Arslanoğlu S et al (2017) Clinical factors associated with the diagnosis of granulomatosis with polyangiitis. Otolaryngol Head Neck Surg 156:484–488

Ernst A, Majid A, Feller-Kopman D et al (2007) Airway stabilization with silicone stents for treating adult tracheobronchomalacia. Chest 132:609–616

Euler U, Liljestrand G (1946) Observations on the pulmonary arterial blood pressure in the cat. Acta Physiol Scand 12:301–320

Fetita CI, Preteux F, Beigelman-Aubry C, Grenier P (2004) Pulmonary airways: 3-D reconstruction from multislice CT and clinical investigation. IEEE Trans Med Imaging 23:1353–1364

Gilkeson RC, Ciancibello LM, Hejal RB et al (2001) Tracheobronchomalacia. Am J Roentgenol 176:205–210

Grenier PA, Beigelman-Aubry C, Fetita C, Martin-Bouyer Y (2003) Multidetector-row CT of the airways. Semin Roentgenol 38:146–157

Gruden JF, Webb WR (1993) CT findings in a proved case of respiratory bronchiolitis. Am J Roentgenol 161:44–46

Hasegawa I, Boiselle PM, Raptopoulos V, Hatabu H (2003) Tracheomalacia incidentally detected on CT pulmonary angiography of patients with suspected pulmonary embolism. Am J Roentgenol 181:1505–1509

Hein E, Rogalla P, Hentschel C et al (2000) Dynamic and quantitative assessment of tracheomalacia by electron beam tomography: correlation with clinical symptoms and bronchoscopy. J Comput Assist Tomogr 24:247–252

Helbich TH, Heinz-Peer G, Eichler I et al (1999) Cystic fibrosis: CT assessment of lung involvement in children and adults. Radiology 213:537–544

Heussel C, Hafner B, Lill J et al (2001) Paired inspiratory/expiratory spiral CT and continuous respiration cine CT in the diagnosis of tracheal instability. Eur Radiol 11:982–989

Holinger LD (1980) Etiology of stridor in the neonate, infant and child. Ann Otol Rhinol Laryngol 89:397–400

Hussain K, Gilbert S (2003) Tracheopathia osteochondroplastica. Clin Med Res 1:239–242

Jokinen K, Palva T, Nuutinen J (1976) Chronic bronchitis. ORL 38:178–186

Jokinen K, Palva T, Sutinen S, Nuutinen J (1977) Acquired tracheobronchomalacia. Ann Clin Res 9:52–57

Kauczor H-U, Wielpütz MO, Owsijewitsch M, Ley-Zaporozhan J (2011) Computed tomographic imaging of the airways in COPD and asthma. J Thorac Imaging 26:290–300

Kauczor HU, Wolcke B, Fischer B et al (1996) Three-dimensional helical CT of the tracheobronchial tree: evaluation of imaging protocols and assessment of suspected stenoses with bronchoscopic correlation. AJR Am J Roentgenol 167:419–424

Kennedy MP, Noone PG, Leigh MW et al (2007) High-resolution CT of patients with primary ciliary dyskinesia. Am J Roentgenol 188:1232–1238

Khan TZ, Wagener JS, Bost T et al (1995) Early pulmonary inflammation in infants with cystic fibrosis. Am J Respir Crit Care Med 151:1075–1082

Kim Y, Kim YK, Lee BE et al (2015) Ultra-low-dose CT of the thorax using iterative reconstruction: evaluation of image quality and radiation dose reduction. Am J Roentgenol 204:1197–1202

Kuehni CE, Frischer T, Strippoli MP et al (2010) Factors influencing age at diagnosis of primary ciliary dyskinesia in European children. Eur Respir J 36:1248–1258

Kwong JS, Müller NL, Miller RR (1992) Diseases of the trachea and main-stem bronchi: correlation of CT with pathologic findings. Radiographics 12:645–657

Lee KS, Ernst A, Trentham DE et al (2006) Relapsing polychondritis: prevalence of expiratory CT airway abnormalities. Radiology 240:565–573

Letko E, Zafirakis P, Baltatzis S et al (2002) Relapsing polychondritis: a clinical review. Semin Arthritis Rheum 31:384–395

Ley S, Ley-Zaporozhan J, Unterhinninghofen R et al (2006) Investigation of retrospective respiratory gating techniques for acquisition of thin-slice 4D-multidetector-computed tomorgraphy (MDCT) of the lung: feasibility study in a large animal model. Exp Lung Res 32:395–412

Little SA, Sproule MW, Cowan MD et al (2002) High resolution computed tomographic assessment of airway wall thickness in chronic asthma: reproducibility and relationship with lung function and severity. Thorax 57:247–253

Lo P, van Ginneken B, Reinhardt JM et al (2012) Extraction of airways from CT (EXACT'09). IEEE Trans Med Imaging 31:2093–2107

Long FR, Williams RS, Castile RG (2004) Structural airway abnormalities in infants and young children with cystic fibrosis. J Pediatr 144:154–161

Loring SH, O'Donnell CR, Feller-Kopman DJ, Ernst A (2007) Central airway mechanics and flow limitation in acquired tracheobronchomalacia. Chest 131:1118–1124

Lucas JS, Burgess A, Mitchison HM et al (2014) Diagnosis and management of primary ciliary dyskinesia. Arch Dis Child 99:850–856

Maffessanti M, Candusso M, Brizzi F, Piovesana F (1996) Cystic fibrosis in children: HRCT findings and distribution of disease. J Thorac Imaging 11:27–38

Marković I, Puksić S, Gudelj-Gracanin A et al (2016) Granulomatosis with polyangiitis (GPA) limited to upper respiratory tract—a case report. Lijec Vjesn 138:54–56

Marom EM, Goodman PC, McAdams HP (2001) Focal abnormalities of the trachea and main bronchi. Am J Roentgenol 176:707–711

Martinez F, Chung JH, Digumarthy SR et al (2012) Common and uncommon manifestations of wegener granulomatosis at chest CT: radiologic-pathologic correlation. Radiographics 32:51–69

Martinez S, Heyneman LE, McAdams HP et al (2008) Mucoid impactions: finger-in-glove sign and other CT and radiographic features. Radiographics 28:1369–1382

Maskell GF, Lockwood CM, Flower CDR (1993) Computed tomography of the lung in Wegener's granulomatosis. Clin Radiol 48:377–380

Mayer D, Bartz D, Fischer J et al (2004) Hybrid segmentation and virtual bronchoscopy based on CT images. Acad Radiol 11:551–565

Meyer CA, White CS (1998) Cartilaginous disorders of the chest. Radiographics 18:1109–1123

Miller WT, Chatzkel J, Hewitt MG (2014) Expiratory air trapping on thoracic computed tomography. A diagnostic subclassification. Ann Am Thorac Soc 11:874–881

Montaudon M, Berger P, Cangini-Sacher A et al (2007) Bronchial measurement with three-dimensional quantitative thin-section CT in patients with cystic fibrosis. Radiology 242:573–581

Murgu SD, Colt HG (2006) Tracheobronchomalacia and excessive dynamic airway collapse. Respirology 11:388–406

Nakamaru Y, Takagi D, Suzuki M et al (2016) Otologic and rhinologic manifestations of eosinophilic granulomatosis with polyangiitis. Audiol Neurotol 21:45–53

Nakano Y, Wong JC, de Jong PA et al (2005) The prediction of small airway dimensions using computed tomography. Am J Respir Crit Care Med 171:142–146

Niimi A, Matsumoto H, Amitani R et al (2004) Effect of short-term treatment with inhaled corticosteroid on airway wall thickening in asthma. Am J Med 116:725–731

O'Regan A, Fenlon HM, Beamis JF et al (2000) Tracheobronchial amyloidosis. The Boston University experience from 1984 to 1999. Medicine (Baltimore) 79:69–79

Papadopoulos NG, Moustaki M, Tsolia M et al (2002) Association of rhinovirus infection with increased disease severity in acute bronchiolitis. Am J Respir Crit Care Med 165:1285–1289

Puderbach M, Eichinger M, Gahr J et al (2007a) Proton MRI appearance of cystic fibrosis: comparison to CT. Eur Radiol 17:716–724

Puderbach M, Eichinger M, Haeselbarth J et al (2007b) Assessment of morphological mri for pulmonary changes in cystic fibrosis (CF) patients: comparison to thin-section CT and chest X-ray. Investig Radiol 42:715–724

Reinhardt JM, D'Souza N, Hoffman EA (1997) Accurate measurement of intrathoracic airways. IEEE Trans Med Imaging 16:820–827

Reynisson PJ, Scali M, Smistad E et al (2015) Airway segmentation and centerline extraction from thoracic CT—comparison of a new method to state of the art commercialized methods. PLoS One 10:e0144282

Ridge CA, Bankier AA, Eisenberg RL (2011) Mosaic attenuation. Am J Roentgenol 197:W970–W977

Rossi SE, Franquet T, Volpacchio M et al (2005) Tree-in-bud pattern at thin-section CT of the lungs: radiologic-pathologic overview. Radiographics 25:789–801

Sharma A, Gnanapandithan K, Sharma K, Sharma S (2013) Relapsing polychondritis: a review. Clin Rheumatol 32:1575–1583

Sheehan RE, Flint JDA, Müller NL (2003) Computed tomography features of the thoracic manifestations of Wegener granulomatosis. J Thorac Imaging 18:34–41

Shin MS, Jackson RM, Ho KJ (1988) Tracheobronchomegaly (Mounier-Kuhn Syndrome): CT diagnosis. Am J Roentgenol 150:777–779

Standring S (2005) Gray's anatomy: the anatomical basis of clinical practice, 39th edn. Elsevier, Edinburgh

Stark P (1995) Imaging of tracheobronchial injuries. J Thorac Imaging 10:206–219

Stern EJ, Swensen SJ, Hartman TE, Frank MS (1995) CT mosaic pattern of lung attenuation: distinguishing different causes. AJR Am J Roentgenol 165:813–816

Sun M, Ernst A, Boiselle PM (2007) MDCT of the central airways: comparison with bronchoscopy in the evaluation of complications of endotracheal and tracheostomy tubes. J Thorac Imaging 22:136–142

Tiddens HAWM (2002) Detecting early structural lung damage in cystic fibrosis. Pediatr Pulmonol 34:228–231

Trentham DE, Le CH (1998) Relapsing polychondritis. Ann Intern Med 129:114

Trigaux JP, Hermes G, Dubois P et al (1994) CT of saber-sheath trachea. Correlation with clinical, chest radiographic and functional findings. Acta Radiol 35:247–250

Tschirren J (2005) Segmentation and quantitative analysis of intrathoracic airway trees from computed tomography images. Proc Am Thorac Soc 2:484–487

Venkatraman R, Raman R, Raman B et al (2006) Fully automated system for three-dimensional bronchial morphology analysis using volumetric multidetector computed tomography of the chest. J Digit Imaging 19:132–139

Webb W (2006) Thin-section CT of the secondary pulmonary lobule: anatomy and the image—the 2004 Fleischner Lecture. Radiology 239:322–338

Webb W, Müller N, Naidich D (2001) High-resolution CT of the lungs. Lippincott, London

Weibel E, Gomez D (1962) Architecture of the human lung. Use of quantitative methods establishes fundamental relations between size and number of lung structures. Science 137:577–585

Weibel ER (1963) Morphometry of the human lung. Springer, Berlin

Weinheimer O, Achenbach T, Bletz C et al (2008) About objective 3-D analysis of airway geometry in computerized tomography. IEEE Trans Med Imaging 27:64–74

Werner C, Onnebrink J, Omran H et al (2015) Diagnosis and management of primary ciliary dyskinesia. Cilia 4:2

Wielpütz M, Eichinger M, Biederer J et al (2016) Imaging of cystic fibrosis lung disease and clinical interpretation. RöFo 188:834–845

Wielpütz MO, Eberhardt R, Puderbach M et al (2014) Simultaneous assessment of airway instability and respiratory dynamics with low-dose 4D-CT in chronic obstructive pulmonary disease: a technical note. Respiration 87:294–300

Wielpütz MO, Eichinger M, Puderbach M (2013a) Magnetic resonance imaging of cystic fibrosis lung disease. J Thorac Imaging 28:151–159

Wielpütz MO, Eichinger M, Weinheimer O et al (2013b) Automatic airway analysis on multidetector computed tomography in cystic fibrosis. J Thorac Imaging 28:104–113

Woodring JH, Howard RS, Rehm SR (1991) Congenital tracheobronchomegaly (Mounier-Kuhn syndrome): a report of 10 cases and review of the literature. J Thorac Imaging 6:1–10

Zhang J, Hasegawa I, Feller-Kopman D, Boiselle PM (2003) Dynamic expiratory volumetric CT imaging of the central airways: comparison of standard-dose and low-dose techniques. Acad Radiol 10:719–724